Sea-ice decline makes zooplankton stay deeper for longer

Hauke Flores (Hauke.Flores@awi.de)
Alfred-Wegener Institute Helmholtz-Institute for Polar and Marine Research https://orcid.org/0000-0003-1617-5449

Gaelle Veyssiere
British Antarctic Survey

Giulia Castellani
Alfred-Wegener Institute Helmholtz-Institute for Polar and Marine Research

Jeremy Wilkinson
British Antarctic Survey

Mario Hoppmann
Alfred-Wegener Institute Helmholtz-Institute for Polar and Marine Research

Michael Karcher
Alfred-Wegener Institute Helmholtz-Institute for Polar and Marine Research

Lovro Valcic
Bruncin

Astrid Cornils
Alfred Wegener Institute Helmholtz Centre for Polar and Marine Research, Section Polar Biological Oceanography https://orcid.org/0000-0003-4536-9015

Maxime Geoffroy
Center for Fisheries Ecosystems Research, Fisheries and Marine Institute of Memorial University of Newfoundland and Labrador

Marcel Nicolaus
Alfred Wegener Institute for Polar and Marine Research https://orcid.org/0000-0003-0903-1746

Barbara Niehoff
Alfred-Wegener Institute Helmholtz-Institute for Polar and Marine Research

Pierre Priou
Akvaplan NIVA

Katrin Schmidt
Plymouth University https://orcid.org/0000-0002-6488-623X

Julienne Stroeve
University College London https://orcid.org/0000-0001-7316-8320

Article

Keywords:

Posted Date: January 10th, 2023

DOI: https://doi.org/10.21203/rs.3.rs-2436026/v1

Additional Declarations: There is **NO** Competing Interest.

Version of Record: A version of this preprint was published at Nature Climate Change on August 28th, 2023. See the published version at https://doi.org/10.1038/s41558-023-01779-1.

Sea-ice decline makes zooplankton stay deeper for longer

H. Flores[1]*, G. Veyssiere[2]*, G. Castellani[1], J. Wilkinson[2], M. Hoppmann[1], M. Karcher[1,3] L. Valcic[4], A. Cornils[1], M. Geoffroy[5,6], M. Nicolaus[1], B. Niehoff[1], P. Priou[5,7], K. Schmidt[8], J. Stroeve[9,10]

*These authors contributed equally to the work.

Affiliations:

[1]Alfred-Wegener-Institut Helmholtz-Zentrum für Polar- und Meeresforschung, Bremerhaven, Germany

[2]British Antarctic Survey, Cambridge, United Kingdom

[3]O.A.Sys - Ocean Atmosphere Systems GmbH, Hamburg, Germany

[4]Bruncin Observation Systems, Zagreb, Croatia

[5]Centre for Fisheries Ecosystems Research, Fisheries and Marine Institute of Memorial University of Newfoundland and Labrador, St. John's, NL, Canada

[6]Department of Arctic and Marine Biology, The Arctic University of Norway, Tromsø, Norway

[7]Akvaplan-Niva, The Fram Centre, Tromsø, Norway

[8]University of Plymouth, School of Geography, Earth and Environmental Sciences, Plymouth, United Kingdom

[9]University of Manitoba, Centre for Earth Observation Science, Winnipeg, Canada

[10]University College London, Earth Sciences Department, London, United Kingdom

Abstract:
As Arctic sea ice deteriorates, more light enters the Arctic Ocean, causing largely unknown effects on the ecosystem. A novel autonomous bio-physical observatory provided the first record of zooplankton vertical distribution under sea ice drifting across the Arctic Ocean from dusk to dawn of the polar night. Its measurements revealed that zooplankton ascend into the under-ice layer during autumn twilight, following an isolume of 5.5 10^{-4} W m^{-2}. We applied this trigger isolume to IPCC models enabled to incorporate incoming radiation after sunset and before sunrise of the polar night. The models project that, in about three decades, the total time spent by zooplankton in the under-ice layer will be reduced by up to one month, depending on geographic region. This will impact zooplankton winter survival, the Arctic foodweb, carbon- and nutrient fluxes. These findings highlight the importance of processes in the twilight periods for predicting change in high-latitude ecosystems.

MAIN

Introduction

The shrinking and thinning sea-ice cover of the Arctic Ocean allows the sunlight to penetrate deeper into the water column and extend the sunlit period in subsurface waters[1]. The increased light penetration already causes profound changes to key ecosystem functions, such as enhanced primary production in the marginal shelf seas, and a shifting phenology of ice algae- and phytoplankton blooms[2, 3, 4, 5]. The effects of the changing light field on higher trophic levels of the Arctic marine ecosystem, however, are not well understood.

The diel change in light intensity is the primary driver of the largest synchronized movement of organisms on Earth: the diel vertical migration of zooplankton[6] (DVM). Commonly, zooplankton ascend to the surface during the night to feed on plankton, and descend to deeper waters during the day to avoid visual predators. In the polar regions, winter-active zooplankton perform a seasonal vertical migration between greater depths during the polar day and shallow depths during the polar night[7, 8, 9, 10]. Besides DVM, polar lipid-rich zooplankton perform an ontogenetic migration, spending the polar night in deep water to overwinter in dormancy. Vertically migrating zooplankton act as an active biological carbon pump (also called 'lipid pump'[11]), accounting for 25-132% of the gravitational biological carbon pump driven by sinking particulate organic carbon[12, 13]. Furthermore, the foraging success of visual predators, such as fish, marine birds, and mammals, depends on the interplay between the timing and depth range of the zooplankton vertical migration and light penetration depth[14, 15, 16].

Earlier studies using hydroacoustic measurements demonstrated that the vertical migration of Arctic zooplankton is particularly sensitive to low light intensities, but were unable to resolve the top 20 m of the ice-covered ocean[7, 8, 17, 18, 19]. These upper 20 m underneath the sea ice, however, constitute an important habitat for zooplankton, because microalgae growing in sea ice ('ice algae') may provide critical food supply, particularly during the polar night[20, 21]. Increasing light penetration through a thinning sea-ice cover may affect the timing of the seasonal migration of zooplankton into and out of the under-ice layer, and hence the net duration of access to these resources.

Field observations indicate that zooplankton vertical migration often follows a trigger level of light intensity[19]. This trigger level must be measured under ambient conditions without disturbance by noise or light, both of which are typically emitted by human-operated research platforms[18]. Only then, trigger levels can be implemented in coupled sea ice-ocean models to predict the change in the timing of the seasonal migration into and out of the under-ice layer based on future light penetration scenarios. In the polar regions, however, such trigger levels occur in the twilight periods during autumn and spring, i.e. after sunset and before sunrise. Because both models and satellite products wrongly assume zero incoming radiation once the sun is below the horizon, an approach considering light penetration during the twilight periods is necessary to realistically model changes in the seasonal migration of zooplankton under sea ice[22].

To investigate how light intensity controls the vertical migration in the under-ice layer of the Arctic Ocean, we developed an ice-tethered, autonomous bio-physical observatory which drifted across the Central Arctic Ocean (CAO) thousands of kilometres away from any artificial light and noise sources. Using data from this observatory, we investigated the vertical distribution of

zooplankton under sea ice in relation to the diel and seasonal change in light intensity from September 2020 to April 2021. From the analysis of these data, we were able to identify the level of light intensity that triggered vertical migration. In order to predict likely shifts in the timing of zooplankton vertical migration over the next 30 years, we applied this trigger level to future light fields derived from models of the Intergovernmental Panel on Climate Change (IPCC) climate model class with an approach allowing to model the light field under sea ice during the autumn and spring twilight periods. Results allowed us to identify potential risks to the functioning of the high-Arctic ecosystem due to changes in vertical migration patterns.

Results

We deployed a newly-developed autonomous bio-physical observatory on sea ice at the end of the MOSAiC drift experiment with RV *Polarstern* in September 2020 (PS122/5)[23, 24]. This observatory consisted, among other components, of an Acoustic Zooplankton and Fish Profiler (AZFP) measuring acoustic backscatter at 67, 125, 200 and 455 kHz in the top 50 m of the ocean, a radiation station equipped with hyperspectral light sensors measuring irradiance at the ice underside between 350 and 920 nm[25], and a CTD (conductivity, temperature, depth) buoy measuring salinity, temperature, pressure and fluorescence at 5 depth levels below the sea ice (10, 20, 50, 75 and 100 m) (Supplementary Fig. 1, 2). All data from the observatory were transmitted via the Iridium satellite system. After the departure of RV Polarstern on 20 September 2020, the observatory was not exposed to external disturbances by noise, artificial light, or human activity. Between the beginning of the measurements on 18 September 2020 close to the North Pole and the end of the study period on 1 April 2021 north of Greenland, the observatory drifted 1,035 km across the CAO (Fig. 1a).

Observations of zooplankton vertical distribution

Using the AZFP, we observed changes in the depth distribution of scatterers in relation to the seasonal cycle of solar irradiance at 125, 200 and 455 kHz, whereas there was nearly zero backscatter at 67 kHz. During the end and the beginning of the polar day, the bulk of the backscatter was confined below a subsurface backscatter maximum (SBM) between 20 and 30 m depth, and the water above the SBM was virtually void of scatterers (Fig. 1b). Once the sun set and true darkness prevailed, most of the backscatter was concentrated between the SBM and the ice underside (Fig. 1, Fig. 2).

During the twilight period following the autumn equinox (22 September 2020), our data showed an eight-day long period of pronounced DVM across the SBM (Fig. 2). At 455 kHz, the average integrated backscatter (s_A) above the SBM varied between about 40 m^2 nmi^{-2} at the diel solar minimum and less than 10 m^2 nmi^{-2} at the diel solar maximum (Fig. 2 a). During the twilight period preceding the spring equinox (22 March 2021), a diel migration pattern was again visible at 455 kHz (Fig. 2 b), but very low acoustic backscatter impeded the detection of diel patterns in the higher frequencies (Supplementary Fig. 4). In general, backscattering strength was consistently strongest at 455 kHz and weakest at 125 kHz, suggesting that the scattering was caused predominantly by similar-sized copepods[10] throughout the observation period. Zooplankton sampling prior to the deployment of the autonomous observatory indicated that the late copepodite stages and females of *Metridia longa* and *Calanus* spp. dominated the zooplankton biovolume in the top 50 m under the sea ice (Supplementary Fig. 5).

Trigger level of light intensity

To determine a level of light intensity triggering DVM during the twilight period, we estimated the light intensity when the zooplankton first migrated across the SBM, which occurred on 28 September 2020. By extrapolating from light measurements at the ice underside into the water column using an exponential decay of light with depth that was measured at the site (attenuation coefficient $K_w = 0.11\ m^{-1}$), we determined the light level when the zooplankton first migrated across the SBM at about 25 m depth. According to this analysis, scatterers crossed the SBM as soon as the light intensity above the SBM decreased below $5.5\ 10^{-4}\ W\ m^{-2}$. The scatterers timed their vertical migration to always stay exactly below this trigger isolume, performing DVM while following the isolume's up and down with the diel light cycle (Fig. 2 c). Once the trigger isolume reached the ice underside on 8 October 2020, high backscatter remained distributed in the under-ice layer between about 10 m depth and the SBM until the spring twilight period.

Future scenarios

As a proxy for the expected mid-21st century shift in the onset of autumn and spring DVM, we calculated the difference (in days) between the mean date when the trigger isolume reaches 25 m depth in the 10-year period 2015-2024 and the 2045-2054 period. The depth of the trigger isolume was estimated based on light transmitted through sea ice and snow calculated from four different IPCC CMIP6 models for the greenhouse gas emission scenarios RCP2.6 and RCP8.5, respectively (Figure 3, 4; Table 1; Supplementary Figs. 6-17). To derive the light levels when the sun was below the horizon, we used twilight downwelling irradiance calculated with the radiation scheme of Spitschan et al. (2016)[22], corrected for solar angle.

Based on increased light penetration due to changes in the sea ice and snow cover, the four IPCC models projected significant shifts of the onset of autumn and spring DVM in the surface waters for large parts of the Arctic Ocean. We plotted the projected shifts on continuous pan-Arctic maps (Fig. 3, 4), and calculated mean shifts (± standard deviation) for 8 Large Marine Ecosystems defined by the Arctic Council Working Group for the Protection of the Arctic Marine Environment (PAME)[26] (Table 1). In both seasons and both greenhouse gas scenarios, the southern Beaufort and Chukchi Seas exhibited the largest shifts (Figs. 3, 4, Table 1). In some regions the simulated internal variability gave rise to a large spread of the model ensembles, reflected in greater standard deviations (Supplementary Figs. 6-7). We defined the projected mean shifts as 'robust' if the ratio of the mean shift to the standard deviation ≥ 2 (Table 1). For autumn, the models for RCP2.6 predicted robust positive mean shifts between 3 days in the Barents Sea and 11 days in the East Siberian Sea, and for RCP8.5 between 1 day in the Barents Sea and 16 days in the East Siberian Sea (Table 1). Notably, in the RCP8.5 scenario robust positive shifts of 6 to 10 days were predicted for the CAO, although it was not the most impacted region. Projected robust changes for spring showed a negative shift of the DVM onset to an earlier date between 1 day in the CAO and 6 days in the East Siberian Sea for RCP2.6, and between 1 day in the Beaufort Sea and 11 days in the Barents Sea for RCP8.5 (Fig. 4; Table 1). In spring, standard deviations in those regions with the highest projected shift were also high due

to a large ensemble spread, indicating that predictions in these regions were associated with greater uncertainty (Supplementary Fig. 7).

Discussion

Our simultaneous observations of zooplankton vertical migration and measured light intensities in the Central Arctic Ocean revealed that in the autumn twilight period still sufficient light penetrated the sea ice to control the DVM of zooplankton after the sun had set. This indicates that the timing of the DVM phase marking the seasonal vertical migration of zooplankton at the beginning and the end of the polar night is highly sensitive to predicted increases in light penetration[1]. The DVM was likely further enhanced by the endogenous circadian clock of zooplankton, as indicated by the continuation of a quasi-synchronous pattern after the trigger isolume had reached the ice underside[27] (Figure 2 c). The trigger level of 5.5 10^{-4} W m^{-2} is within the order of magnitude assumed to trigger negative phototaxis in crustacean zooplankton[28]. In a hydroacoustic study in the ice-free Kongsfjorden, Hobbs et al. (2021)[19] found that the DVM of zooplankton followed a trigger level of 10^{-7} µmol photons m^{-2} s^{-1}, which had been experimentally determined in female *Calanus* spp. for certain wavelength bands[29]. Converted to photon flux per wavelength band, our trigger level at 530 nm ranges at 8.89 10^{-6} µmol photons m^{-2} s^{-1}, which is very close to the experimentally determined value for this wavelength[29] (see online methods).

DVM is often explained by a trade-off between access to food in the surface layer and predation risk[6]. The darkness of the high-Arctic polar night allows zooplankton to exploit resources from the under-ice habitat without added predation risk. Accordingly, the winter-active copepod *Metridia longa* resides in surface layer during winter while dwelling at depth >100 m during summer[30, 31]. Likewise, parts of the population of *Calanus* spp. remain active in the surface layer during the polar night in the Central Arctic Ocean, whereas the bulk of the population overwinters at greater depths[32]. During the autumn twilight period, our *chlorophyll-a* fluorescence measurements indicated that some phytoplankton was still available for grazers in the under-ice layer, but fluorescence steadily declined towards zero by mid-October (Supplementary Fig. 2). During the polar night, organic matter produced by ice algae when sufficient light was still available may constitute a critical ‘sea-ice food bank’, from where carbon is transferred into the water column by ice-associated organisms and organic particles released by brine rejection[33, 34, 35]. We suggest that this particle rain and its associated microfauna provide low but critical amounts of carbon necessary to satisfy the energy demand of winter-active zooplankton[21, 36, 37, 38, 39]. Furthermore, observations from the CTD buoy suggest that the persistent SBM at 20-30 m depth was probably associated with a strong pycnocline[40] which retained food for zooplankton in the under-ice layer (Supplementary Fig. 3).

Projections of future changes in the timing of DVM onset in spring and autumn were based on the output from a subset of four IPCC model ensemble experiments from CMIP6. These had provided reasonable sensitivity of the sea ice cover to greenhouse gas forcing[41]. However, the results of the model-based projections are still subject to various sources of uncertainty, e.g. model performance and natural variability[41]. Notably, most of the models tend to under-estimate

present-day sea-ice thickness and to overestimate present-day sea-ice concentration in the marginal ice zones. This bias is strongest in the regions with the thickest sea ice north of the Canadian and Greenland coast in the Canadian Archipelago region, which were not the areas of focus in this study. Because we limited our study to the effect of changes in sea ice and snow on the light regime for which reliable IPCC-class models exist, we did not consider uncertainty derived from other potential changes that can affect the light regime in the future, such as a changed cloud cover or changed albedo. Based on our assessment of the variability of model outcomes across all ensemble members in each of the four models, the range of robust shifts of the onset of DVM (e.g., RCP 8.5: 1 to 16 days in autumn and -1 to -11 days in spring) covers the most likely range of future scenarios, considering the above-mentioned sources of model uncertainty (Table 1). We note, however, that within all 4 models each ensemble member represents a possible reality predicted by its model. Therefore, in some regions extreme positive and negative shifts outside the standard deviations shown in Table 1 cannot be excluded, although they are not supported by the majority of the models and thus less likely (Supplementary Tables 3, 4).

In the period 2045 to 2055, the peak of the spring phytoplankton bloom is expected to be several weeks earlier compared to the present[4]. According to a model study by Tedesco et al. (2019)[3], the spring ice algae bloom north of 80°N will be much more productive (up to 2,500% increase in gross primary production), but it will peak about 6 weeks earlier in the second half of this century compared to the present and will have vanished before the end of summer due to ice melt. Hence, in spite of increased productivity, delayed seasonal upward migration of zooplankton at the onset of the polar night further increases a gap between the peak blooms of phytoplankton and ice algae in early summer and the arrival of zooplankton in the under-ice layer in autumn. Furthermore, delayed new-ice formation will largely limit the production of new biomass by ice algae in autumn[42], leading to lower carbon stocks in the 'sea-ice food bank' during the polar night (Fig. 5). These effects reduce the survival probability of winter-active zooplankton, because they enter the polar night with lower energy reserves, and will likely find less ice-associated organic matter in the under-ice layer[2, 3, 43] (Fig. 5). In springtime, earlier seasonal downward migration may impact on the ecologically important copepod *Calanus hyperboreus*. Female *C. hyperboreus* spawn at depth during winter, and the early nauplius larvae rise to the surface, while growing into larger copepodite stages[44, 45]. An earlier descent of omnivorous copepods such as *Metridia* spp. can lead to increased predation on *C. hyperboreus* nauplius larvae before they have outgrown the prey size range of *Metridia* spp, compromising the recruitment of *C. hyperboreus*[46] (Fig. 5). Furthermore, a shorter period of the presence of zooplankton in the under-ice layer may also have cascading effects on higher trophic levels, such as the ecological key species polar cod *Boreogadus saida*, which prey on zooplankton at the ice-water interface[47, 48].

The application of a fully autonomous bio-physical observatory enabled us to monitor animal behaviour under sea ice during its drift across the CAO, a task which has so far required immense logistic effort and therefore left considerable knowledge gaps regarding higher trophic levels in the Arctic ecosystem[49]. Similar technology will be important for understanding changes

of the future Arctic ecosystem and its management, e.g. under the Central Arctic Ocean Fisheries Agreement (CAOFA). Furthermore, by modeling twilight conditions at the beginning and the end of the polar night, our results show for the first time that future changes of the under-ice light field will significantly impact on the timing of the seasonal vertical migration of zooplankton. These changes suggest several ecological risks for key species, their related ecosystem functions and biodiversity. This implies that considering biological processes during the twilight periods would be an important factor determining our ability to predict whether the CAO will become a "new oasis" or a "desert"[4], if the climate crisis cannot be controlled.

ONLINE METHODS

Autonomous bio-physical observatory

We deployed an autonomous bio-physical observatory on the ice floe of the MOSAiC expedition of RV *Polarstern* in September 2020 (PS122/5). This observatory made it possible to investigate the distribution of zooplankton in the top 50 m under the drifting sea ice in relation to environmental parameters, without introducing disturbance by invasive sampling gear or light. The main component was a newly designed Acoustic Zooplankton Fish Profiler (AZFP) buoy which recorded zooplankton vertical distribution from the autumn-winter transition close to the geographic North Pole on 18 September 2020 to the winter-spring transition north of Greenland on 1 April 2021. These measurements were complemented by under-ice irradiance and oceanographic measurements obtained from several co-deployed platforms.

AZFP buoy

An Acoustic Zooplankton and Fish Profiler (AZFP; ASL Environmental Sciences, Victoria, Canada) was integrated into a rugged sea-ice tethered buoy designed to survive the harsh conditions of the ice-covered ocean by Bruncin d.o.o. za usluge (Croatia). The surface unit of the buoy was composed of a heavy metal cylinder housing the batteries, a solid frame carrying the main electronics, a glass half-dome with solar panels, and a stable floatation body around the main hull. The buoy was powered by alkaline batteries sufficient for several months of operation, complemented by a solar-rechargeable power supply to support a higher sampling interval during summer. The surface unit was equipped with additional sensors, including GPS position, under-ice fluorescence, temperature, salinity and cameras (Supplementary Table 1). The underwater unit mainly consisted of the AZFP with its 4 downward-looking acoustic transducers, mounted in a frame fixed to the bottom of the battery cylinder with multiple steel wires and hanging just beneath the ice base (Supplementary Fig. 1). The buoy was running on a Linux operating system, configured to poll the entire sensor suite at regular intervals, and to transmit the recordings to a land-based station via the Iridium satellite network. AZFP sampling parameters and measurement intervals could be adjusted via a remote satellite connection at any time. The buoy was installed on the MOSAiC ice floe on 12 September 2020, in a hydro-hole through 1.3 m thick level ice.

The AZFP recorded acoustic backscatter of zooplankton and fish in the water column at four frequencies: 67, 125, 200 and 455 kHz. In this study, we present data from the 125, 200 and 455 kHz transducers. These frequencies are suitable to detect copepods and other mesozooplankton[10, 50]. The manufacturer calibrated all frequencies of the AZFP before deployment (± 1 dB re 1m-1). The transducers had a nominal -3dB beam angle of 10˚ at 67 kHz, 8˚ at 125 and 200 kHz, and 7° at 455 kHz. The pulse length was set to 500 µs, and the ping rate was 0.5 Hz in all frequencies. Measurements were averaged over burst periods of 2 minutes and a vertical cell height of about 0.5 m.

The AZFP buoy was fully operational on 18 September 2020. The last data transmission was recorded on 7 May 2021. For the purpose of this study, we limited the data to the period from the

start of the twilight period at the end of the polar day on 18 September 2020 (89.1°N 107.4°E) to the end of the twilight period at the end of the polar night on 1 April 2021 (84.6°N 22.3°W). During this period, the observatory was mainly drifting over the Arctic Basin.

To maintain sufficient battery power, we applied an adaptive interval scheme. At the start of the survey on 18 September 2020, AZFP measurements were conducted every 2 hours for a period of 20 minutes (10 bursts), and for 10 minutes (5 bursts) after 30 September 2020 (Supplementary Table 2). To save battery power during darkness, the interval between measurements was set to 12 hours between 19 and 29 October 2020, and the measurement duration was increased to 20 minutes on 20 October 2020 (Supplementary Table 2). After 29 October 2020, the interval between measurements was set to 3 hours, and the duration of measurements was reduced to 6 minutes (3 bursts). To maintain sufficient battery power until the end of the winter, the interval between measurements was further increased to 4 hours on 12 January 2021(Supplementary Table 2). The hydroacoustic data of the AZFP buoy have been submitted to the PANGAEA repository.

Hydroacoustic data processing

Acoustic data were processed with Echoview 12 (Echoview Software Pty Ltd.). We used Echoview's built-in algorithm to remove background and impulse noise, applying a minimum signal-to-noise ratio of 10[51, 52]. In addition, echograms were visually inspected for bad data regions and artifacts, which were manually removed. Data were expressed as volume backscattering strength (S_V in dB re 1 m^{-1}) for each measurement cell (~ 0.5 m * 2 min) between 1 m below the ice and 50 m depth. Initial data exploration revealed the presence of a pronounced subsurface backscatter maximum (SBM) between about 20 and 30 m depth, which persisted from the beginning of the measurements until mid-March 2021 (Fig. 1). This SBM corresponded to a strong difference in salinity between CTD sensors positions above and below the SBM and a strong density gradient (Supplementary Fig. 2, 3), indicating that the elevated backscatter could have been related to both the impedance by the pycnocline and the aggregation of zooplankton at the pycnocline[40]. The overlap of potential zooplankton backscatter with halocline-related backscatter did not compromise observations of the relative shifts in the vertical distribution of scatterers. For the analysis of DVM in the twilight periods (Fig. 2 a,b, Supplementary Fig. 4), we integrated the backscatter data in 2 min long cells reaching from 1 m depth to approximately 2 m above the SBM. For each integration cell, we calculated the nautical area scattering coefficient (s_A in m^2 nmi^{-2}). Data analysis and graphical presentation was conducted in R (version 3.6.1[53]).

Radiation station

A spectral radiation station consisting of 3 spectral radiometers (RAMSES-ACC-VIS, TriOS GmbH, Germany) was installed ~50 m from the AZFP buoy on 27 August 2020. The upward-looking main sensor was installed immediately below the ice base of a refrozen melt pond to measure transmitted irradiance. The sensor also carried an inclination and pressure module. A second sensor was installed above the surface to measure incident irradiance as a reference. An external tiltmeter was attached to the sensor. The station also carried a third radiometer measuring reflected irradiance, a light chain to measure in-ice light attenuation, a snow pinger to

measure snow accumulation and a camera to monitor the state of the observatory (not used here). The radiation station stopped operating on 13 November 2020. The data of the radiation station are available at https://doi.pangaea.de/10.1594/PANGAEA.948838[54].

CTD buoy

Water column structure was recorded and transmitted via the Iridium satellite network by a buoy equipped with 5 SBE37IMP Microcat CTDs (Sea-Bird Scientific, Bellevue, USA) at 10, 20, 50, 75 and 100 m depth along an inductive modem tether. The buoy itself was built by Pacific Gyre, California, USA. It was deployed at a location ~120 m from the AZFP buoy on 28 August 2020. The transmission interval was set to 10 minutes. A more detailed description of the buoy is given in Hoppmann, 2022[55]. The data of this buoy are available online at https://data.meereisportal.de/[56] and are currently being archived in PANGAEA.

Zooplankton sampling

On 16 September 2020 at station PS122/5_62-71 of the MOSAiC expedition, the epipelagic zooplankton community was sampled vertically from 50 m depth to the surface (Hydrobios Multinet Midi; 150µm mesh size, 0.25 m^2). The multinet was equipped with an electronic flow meter measuring the amount of filtered water in m^3 for each sample. Immediately after sampling, the animals were preserved in a 4% formaldehyde-seawater solution buffered with hexamethylenetetramine, and stored at room temperature until quantitative analysis at the Alfred-Wegener-Institute using the scanning system ZooScan[57] (Biotom, Hydroptic, France). The sample was size-fractionated by sieving over 70 µm, 500 µm and 1000 µm meshes to avoid overlapping large and small organisms on the scanner. The size fractions were then scanned with a resolution of 2400 dpi. The resulting scan was processed and separated into images with single objects with ZooProcess, a macro in ImageJ. Length and width of each individual (major axis, minor axis) were automatically measured. The single object images were uploaded to EcoTaxa[58], a web application for the semi-automatic taxonomic classification of the images and sorted into taxonomic categories. Assuming each object to be an ellipsoid, the volume (mm^3) of each zooplankton individual was calculated using the formula:

$$V = \frac{4\pi}{3} \cdot \frac{a}{2} \cdot \left(\frac{b}{2}\right)^2 \qquad (1),$$

Where V is the volume of an organism, a is the major axis, and b is the minor axis. The biovolume of each taxonomic category was then calculated as the sum of all such individual volumes divided by the amount of filtered water of each sample ($mm^3\ m^{-3}$).

Modeling under-ice light field and projecting shift of DVM onset

Calculation of level of light intensity triggering vertical migration

To estimate the level of light intensity triggering the autumn diel vertical migration (DVM) of zooplankton into the under-ice layer above the SBM, we first identified the date when DVM crossed the SBM as 28 September 2020, based on a rise in the integrated nautical area scattering coefficient in the under-ice layer above the SBM (Fig. 2a). Then, we used the measured under-

sea-ice irradiance data from the radiation station and propagated it into the water column using an exponential decay following:

$$I_w = I_{ui} \cdot \exp(-k_w \cdot d_z) \qquad (2),$$

where I_w is the light intensity in W m^{-2} transmitted into the water column, I_{ui} is the under-ice light intensity measured by the radiation buoy, k_w is the water attenuation coefficient, and d_z is the incremental depth in m. To propagate the irradiance transmitted through sea ice into the water column, we calculated the attenuation in the water from data collected by a Remotely Operated Vehicle (ROV)[59] during MOSAiC on 17 September 2020[60]. The attenuation coefficient in the water was averaged over the first 25 m depth and estimated as 0.11 m^{-1}. We provide the trigger level as irradiance (W m^{-2}) as well as photosynthetic photon flux density (PPFD, µmol photons m^{-2} s^{-1}). For the irradiance, we considered the visible part of the spectrum (400-700 nm) from the measurements. For the PPFD, the trigger level was first estimated in W m^{-2} considering the total spectrum available (320-950 nm), and then converted into µmol photons m^{-2} s^{-1} following Castellani et al. (2017)[61]. The resulting light level at the depth of the SBM when DVM began (25 m) was 5.5 10^{-4} W m^{-2} or 1.4 10^{-3} µmol photons m^{-2} s^{-1}. We then plotted the evolution of this trigger level as a function of time and depth (isolume) with the backscatter data (Fig. 2c). In addition, we provide the light threshold for two single wavelengths in the blue part of the spectrum (455 nm) and the green part of the spectrum (530 nm) in order to compare our results with previous studies. The light thresholds for 455 nm and 530 nm were 1.41 10^{-5} µmol photons m^{-2} s^{-1} and 8.89 10^{-6} µmol photons m^{-2} s^{-1}, respectively.

Modeling

As a proxy of the expected mid-21st century shift in the onset of autumn and spring DVM, we calculated the difference (in days) between the mean dates when the trigger isolume reaches 25 m depth in both seasons for the 10-year period 2015-2024 and the 2045-2054 period, respectively. The projected shifts were determined considering future sea-ice concentration, sea-ice thickness, and snow depth. To achieve this, we used model outputs based on the greenhouse gas emission scenarios RCP2.6 and RCP8.5 experiments for the 10-year periods 2015-2024 and 2045-2054 from four different IPCC CMIP6 model ensembles. The model experiments used in this study have shown a reasonable climate change-driven sea-ice loss compared to the change in global mean temperature[41]. Further selection criteria were the availability of daily outputs and of multiple ensemble members. The models were (number of ensemble members in brackets): ACCESS-CM2 (4)[62], MPI-ESM1-2-HR (2)[63], MPI-ESM1-2-LR (29)[64], MRI-ESM2-0 (5)[65]. Decadal means for the periods 2015-2024 and 2045-2054 were calculated for sea-ice concentration, sea-ice thickness and snow depth for each ensemble member for the autumn-winter transition (September to November) and winter-spring transition (January to March). All ensemble members of each of the model scenario experiments were used to accommodate for internal model variability (Supplementary Fig. 8-17).

Downwelling shortwave radiation at the surface was taken from the Clouds and the Earth's Radiant Energy System (CERES) synoptic satellite-based products[66]. These products were

available daily, at a 1° by 1° resolution over the Arctic Ocean and from instruments on board the Terra and Aqua satellites. Because future downwelling radiation is unknown, and our investigation focuses on the relative effect of future sea ice and snow conditions predicted by climate model experiments, we used observed downwelling radiation for the period 1 September to 30 November 2020 and 1 January to 31 March 2020 for all years. As twilight and night light levels of downwelling shortwave radiation are not provided by this remote sensing dataset, we used twilight downwelling irradiance estimates based on the 'Commission Internationale de l'Eclairage (CIE)' daylight model, extended with implemented supplementary basic functions based on field measurements[22]. For the purpose of this study, we calculated incoming solar spectra for sun angles between -28° and 0° at a 2° resolution. The broadband albedo was calculated based on observations during the SHEBA ice drift experiment and considered constant at 0.84[67].

The light transmission through snow and sea ice was calculated using an exponential decay of light through snow and sea-ice using varying extinction coefficients based on physical conditions[5]. With this approach, snow depth and sea-ice thickness sub-grid scale distributions are applied to account for the variability within each grid cell. For the water column, we applied the extinction coefficient determined during the MOSAiC expedition (Kw=0.11 m^{-1}). Then, we calculated the depth profiles of transmitted light into the water column in each grid cell of the 25-km EASE-grid, averaged for the 2015-2024 and the 2045-2054 decades, respectively. These datasets were used to determine the Julian day at which the trigger level of 5.5 10^{-4} W m^{-2} (1.4 10^{-3} µmol photons m^{-2} s^{-1}) is reached at a depth of 25 m in autumn and spring, respectively. The average ensemble values, standard deviations, minimum and maximum for each model in the different Arctic Large Marine Ecosystems (LMEs)[26] displayed in Table 1 and Supplementary Tables 3 and 4 were estimated using the Arctic mask shown in Supplementary Figure 18.

FIGURES

Fig.1: Acoustic backscatter during the drift of the observatory

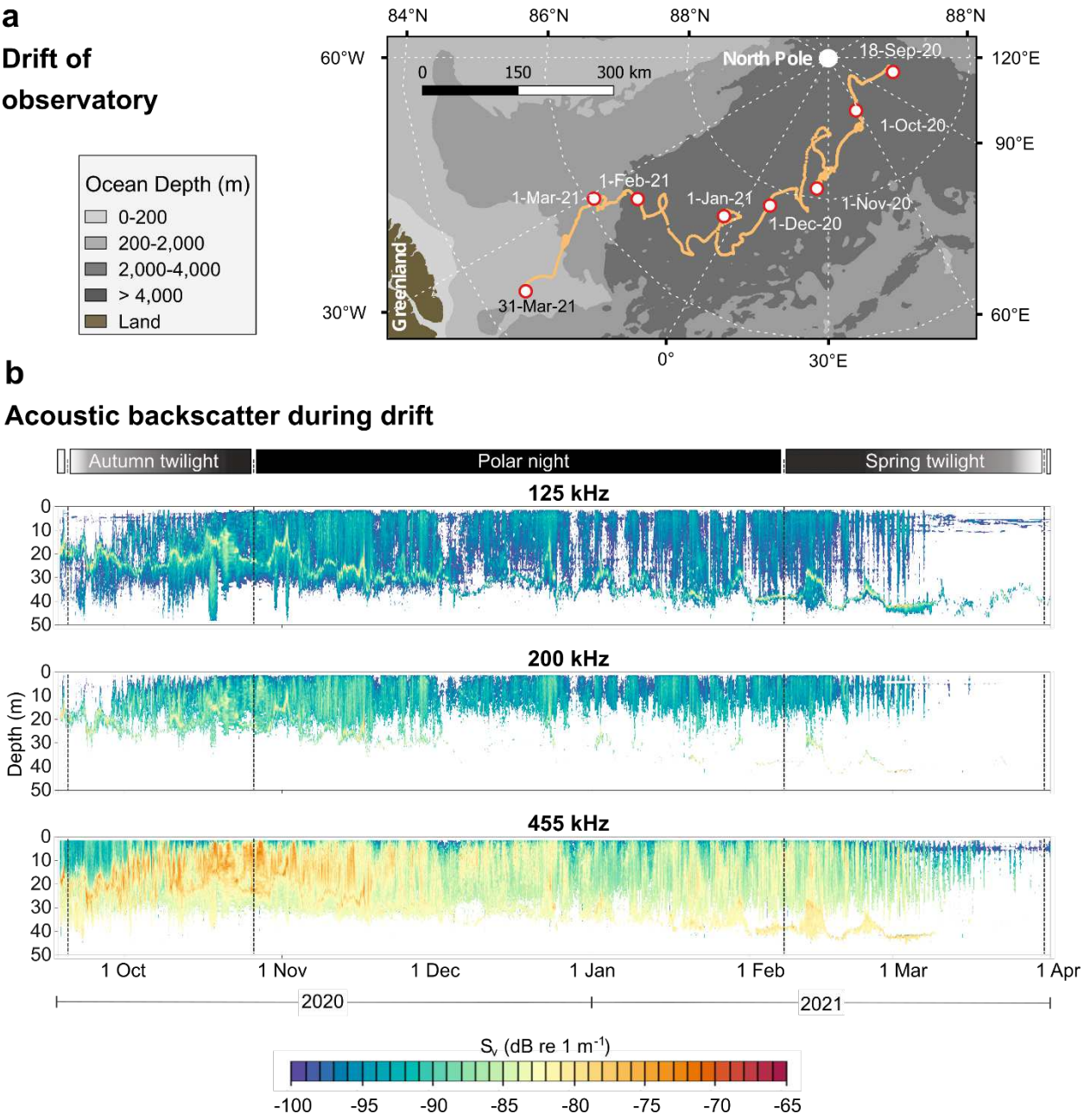

Fig. 1. a, Drift of the autonomous sea ice observatory in the central Arctic Ocean. Monthly drift positions are indicated as white dots with red outline. Bathymetry: International Bathymetric Chart of the Arctic Ocean (IBCAO) Ver. 4.0[68]. **b,** Time series plot of mean volume backscattering strength (S_v) at 125, 200 and 455 kHz, for the entire observation period. The dashed vertical lines indicate (from left to right) the approximate dates of the first day of the autumn nautical twilight period, the beginning of the polar night, the end of the polar night, and the last day of the spring nautical twilight period.

Fig. 2: Diel vertical migration during the autumn and spring twilight periods

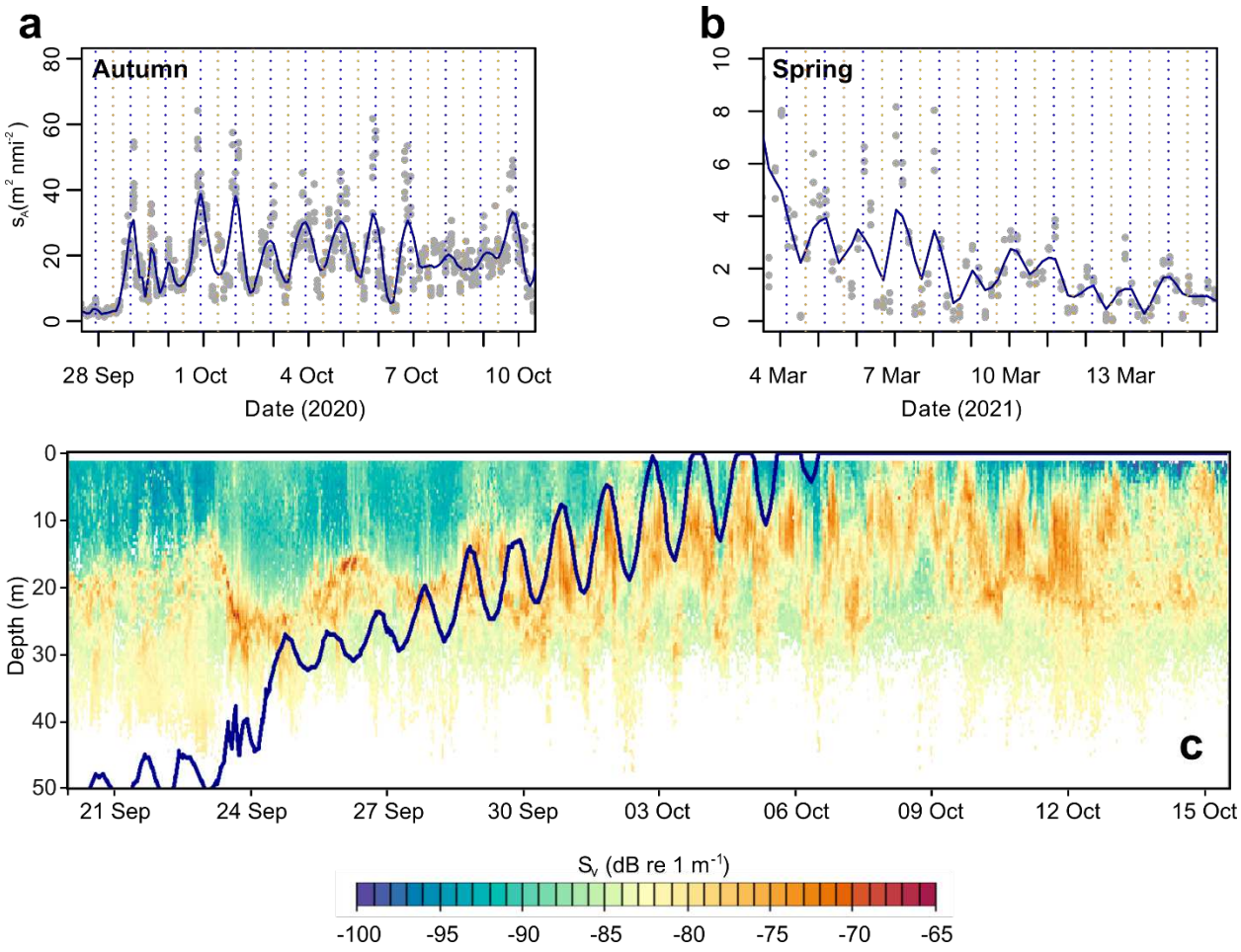

Fig. 2. a-b, Diel variability of the depth-integrated nautical area scattering coefficient (NASC or s_A) during the autumn and spring twilight periods. NASC at 455 kHz above the surface backscatter maximum (SBM) during the autumn (**a**) and spring (**b**) twilight periods. Note the different scales of the x-axis between a and b. Dark blue lines indicate the relative change in s_A during the day estimated by a loess smoother. s_A data are shown as grey dots. Blue vertical hatched lines indicate the time of the daily minimum solar angle, and orange vertical hatched lines indicate time of daily maximum solar angle. **c,** Echogram of the mean volume backscattering strength (S_v) at 455 KHz during autumn twilight. The dark blue line indicates the depth at which the light intensity under the sea ice equals the migration trigger level of 5.5 10^{-4} W m^{-2}.

Fig. 3: Projected mean shift of autumn diel vertical migration onset in mid-21st century compared to present

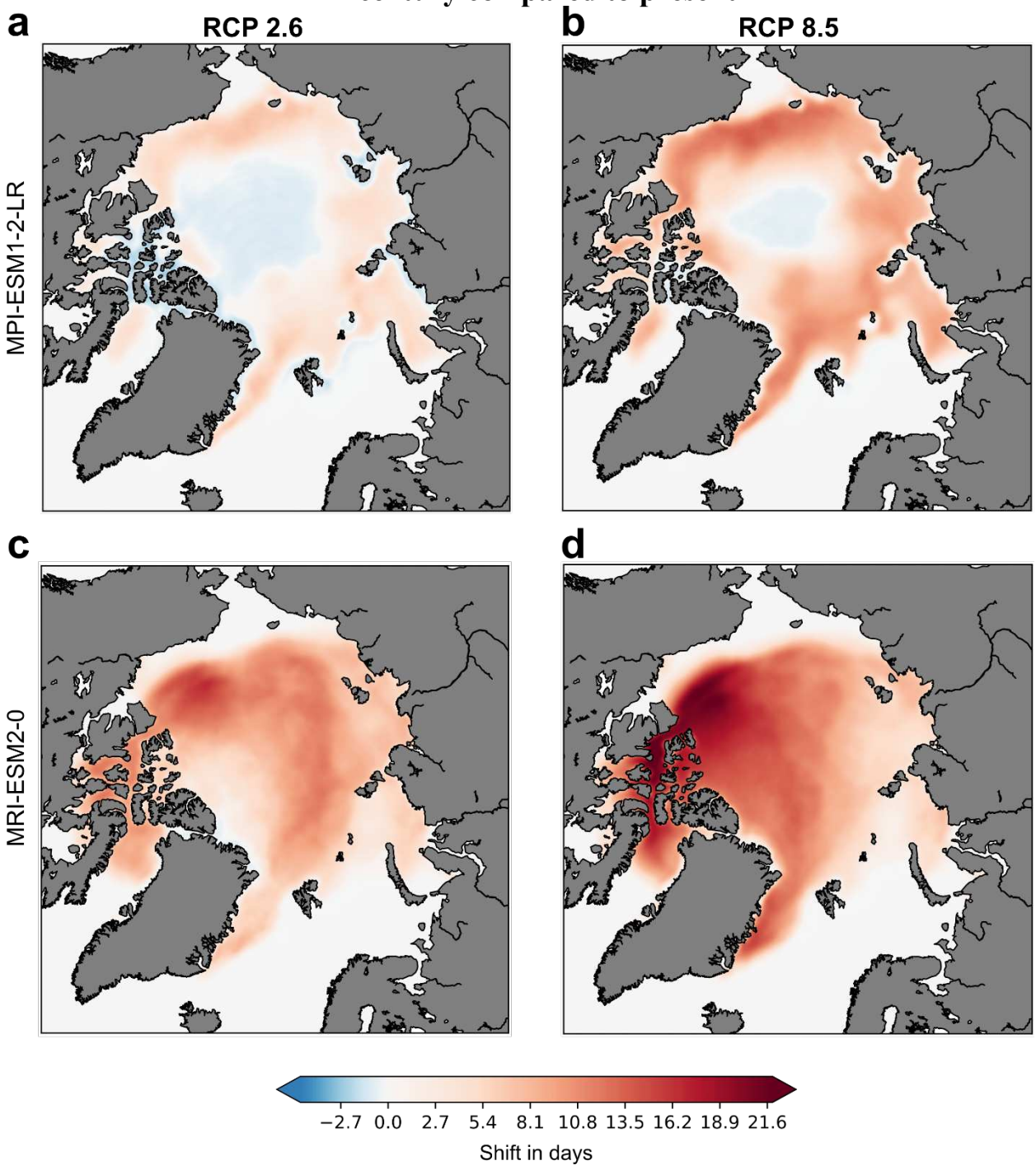

Fig. 3. Pan-Arctic maps of the weakest (**a, b**: MPI-ESM1-2-LR) and strongest (**c, d**: MRI-ESM2-0) predicted average shifts of the autumn DVM onset for the RCP2.6 (**a, c**) and RCP8.5 (**b, d**) scenarios, when contrasting 2045-2054 with the baseline in 2015-2024.

Fig. 4: Projected mean shift of spring diel vertical migration onset in mid-21st century compared to present

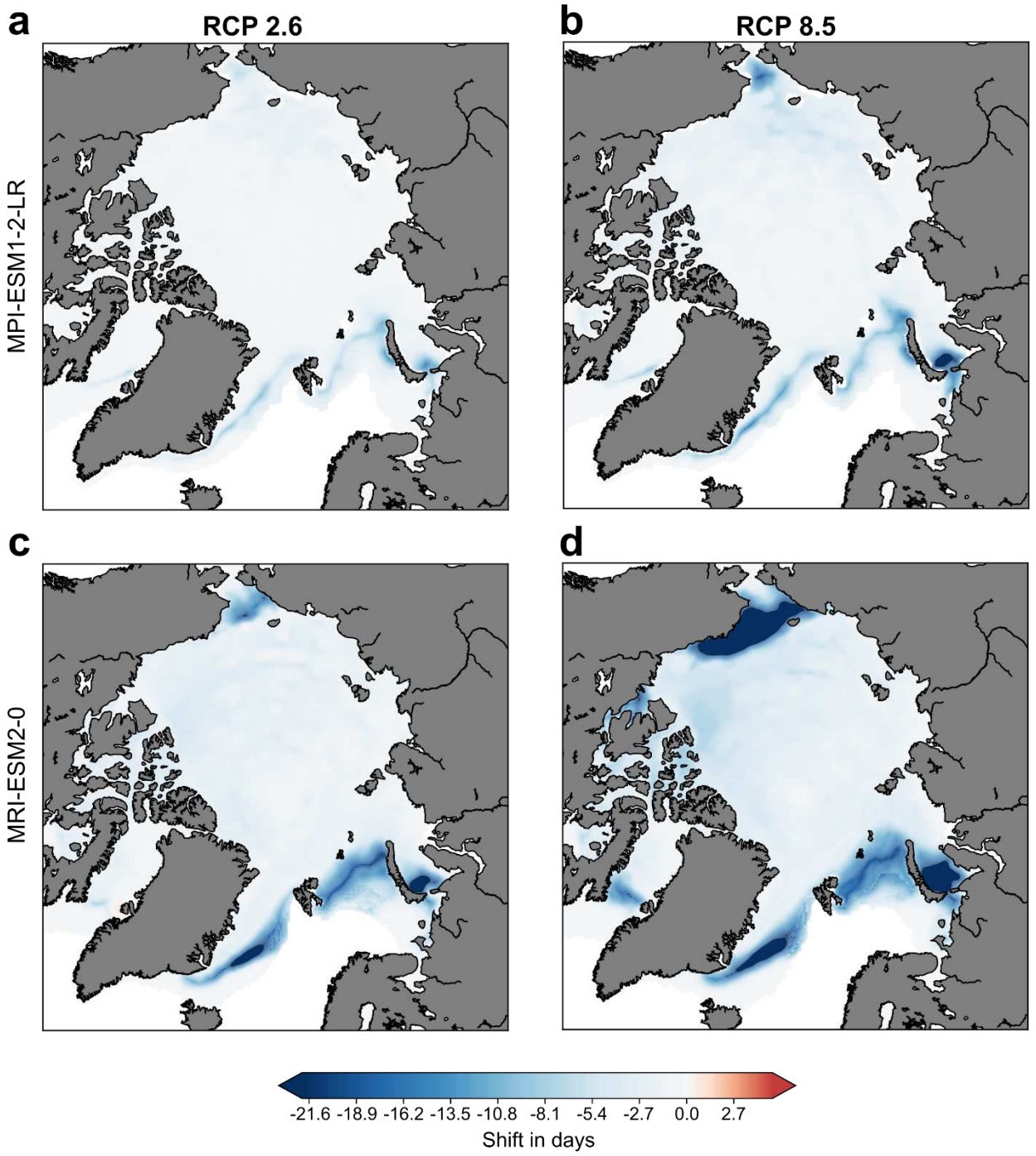

Fig. 4. Pan-Arctic maps of the weakest (**a, b**: MPI-ESM1-2-LR) and strongest (**c, d**: MRI-ESM2-0) predicted average shifts of the spring DVM onset for the RCP2.6 (**a, c**) and RCP8.5 (**b, d**) scenarios, when contrasting 2045-2054 with the baseline in 2015-2024.

Fig. 5: Potential ecological risks of shifts in the timing of seasonal migrations

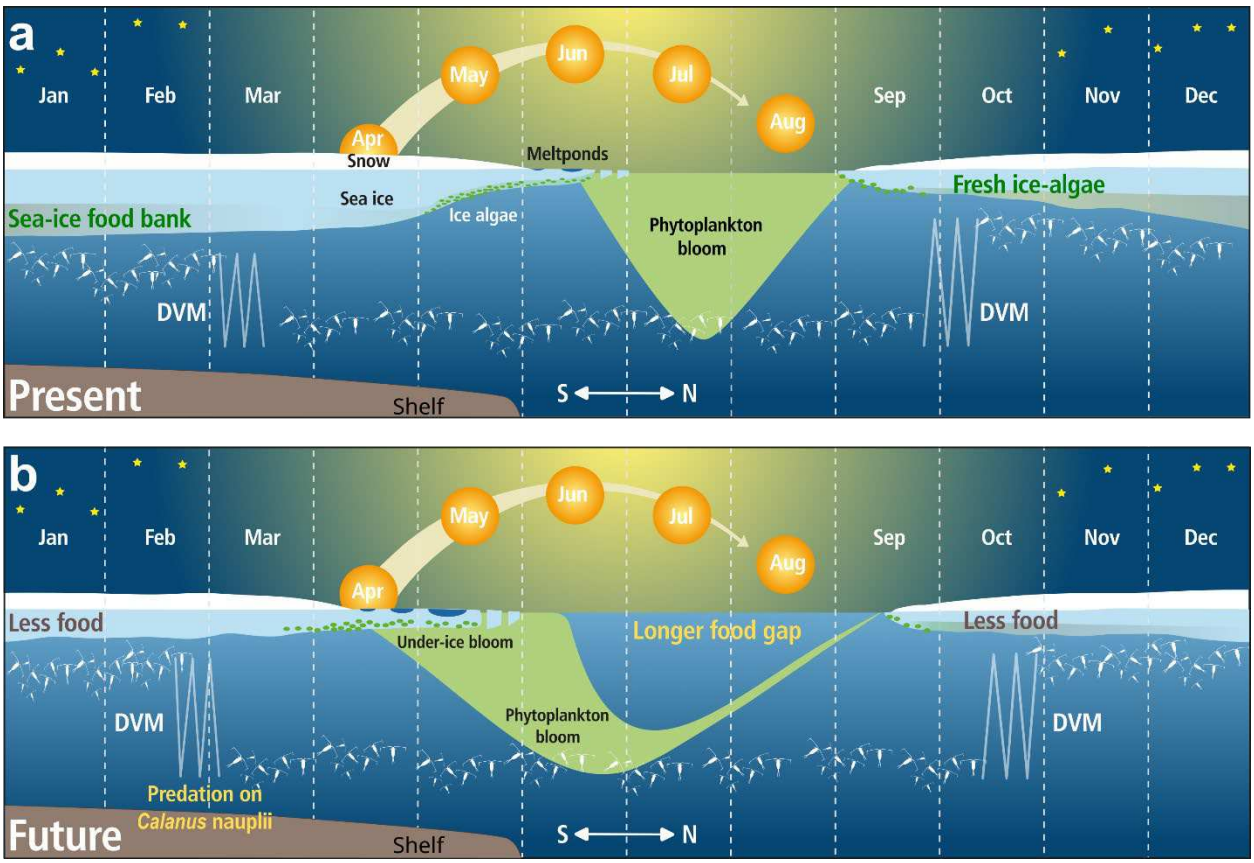

Fig. 5. Present (**a**) and future (**b**) scenarios showing potential ecological risks of negative (spring) and positive (autumn) shifts in the onset of diel vertical migration of zooplankton within the surface layer (0-50 m) of the Arctic Ocean, assuming a 'business-as-usual' (RCP 8.5) scenario. The figure shows a schematic annual cycle with the summer in the centre, along a gradient from shelf seas at low latitudes (< 80°N, left) to the Central Arctic Ocean at high latitudes (> 85°N, right). **a, At present**, zooplankton feed on the phytoplankton bloom during polar day. During the polar night, zooplankton dwelling in the under-ice layer benefit from ice algae-produced carbon stocks, the 'sea-ice food bank'. On the shelf, the springtime downward migration begins after nauplius larvae of the copepod *Calanus hyperboreus* have migrated to the surface and developed to copepodites. **b, In the future**, the springtime downward migration on the shelf may begin so early that omnivorous zooplankton can prey on the developing *C. hyperboreus* nauplii before they ascend[46]. When they migrate into the under-ice layer in autumn, zooplankton may have less carbon available due to a shorter productive period of ice algae. At high latitudes, a longer starvation period between the end of the phytoplankton bloom and the delayed migration into the under-ice layer at the onset of polar night may additionally impact on winter survival of zooplankton. The intensity of the green-brown shading in sea ice symbolizes relative changes in ice algae-produced carbon stocks. The green shading of phytoplankton blooms is not scaled to productivity or biomass. DVM = diel vertical migration during the twilight period. Figure not drawn to scale. This Figure was based on scenarios shown in Soreide et al. (2010)[69], Leu et al. (2011)[43], Wassmann and Reigstad (2011)[2], and Ardyna and Arrigo (2020)[4].

TABLE

Table 1. Mean (± standard deviation) shift of autumn and spring DVM onset in days for Arctic large marine ecosystems (LMEs)[26] for all models when contrasting 2045-2054 with the baseline in 2015-2024 under scenarios RCP2.6 and RCP8.5. For each season, the two models with the lowest and greatest predicted shifts shown in Fig. 3 and Fig. 4 are highlighted in grey shading. Bold numbers indicate 'robust' ensemble mean shifts where the ratio of the ensemble mean shift versus the standard deviation ≥ 2. Map in top left corner shows distribution of LMEs in the Arctic Ocean

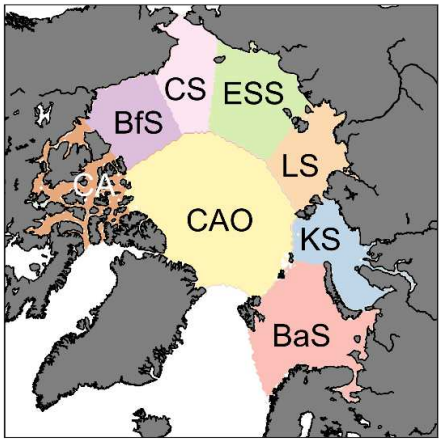

Table 1: Mean shift in onset of diel vertical migration in Large Marine Ecosystems

CA = Canadian Archipelago
BfS = Beaufort Sea
CS = Chukchi Sea
ESS = East Siberian Sea
LS = Laptev Sea
KS = Kara Sea
BaS = Barents Sea
CAO = Central Arctic Ocean

		RCP 2.6				RCP 8.5			
		ACCESS-CM2	MRI-ESM2-0	MPI-ESM1-2-HR	MPI-ESM1-2-LR	ACCESS-CM2	MRI-ESM2-0	MPI-ESM1-2-HR	MPI-ESM1-2-LR
AUTUMN	Chukchi Sea	**10.1 ± 4.9**	**8.4 ± 3.9**	2.7 ± 2.9	3.0 ± 2.7	13.0± 6.7	9.3 ± 5.5	6.5 ± 4.0	7.2 ± 4.5
	Beaufort Sea	7.1 ± 3.9	9.1 ± 5.1	5.7 ± 4.7	2.0 ± 2.1	**11.5 ± 4.9**	13.7 ± 8.1	**9.6 ± 3.9**	**7.0 ± 3.1**
	Canadian Archipelago	2.1 ± 3.0	6.1 ± 3.2	2.1± 3.5	0.8 ± 1.8	5.2 ± 3.9	**14.0 ± 5.2**	4.4 ± 4.3	3.7 ± 2.7
	Central Arctic Ocean	5.1 ± 3.3	**6.6 ± 3.1**	0.8 ± 2.7	0.6 ± 1.7	**10.0 ± 3.4**	**10.2 ± 3.8**	**6.4 ± 2.9**	4.0 ± 3.6
	Barents Sea	4.2 ± 2.5	1.8 ± 1.2	**3.0 ± 1.9**	1.3± 2.1	3.9 ± 2.8	**1.4 ± 0.8**	5.0 ± 3.4	3.8 ± 2.5
	Laptev Sea	**7.2 ± 2.6**	**7.1± 1.4**	3.5 ± 2.5	2.4 ± 1.6	**9.9 ± 3.4**	**4.1 ± 1.1**	**6.7 ± 3.0**	**6.8 ± 2.2**
	Kara Sea	**6.7 ± 3.0**	**3.7 ± 1.5**	3.8 ± 2.2	2.7 ± 1.8	**7.7± 3.2**	2.7 ± 1.5	**6.3± 2.8**	**5.8 ± 2.4**
	E. Siberian Sea	**11.3 ± 3.5**	**8.2 ± 3.2**	2.4 ± 1.7	1.6 ± 2.1	**15.9 ± 3.8**	**7.1 ± 3.3**	**6.9 ± 2.2**	6.0 ± 3.2
SPRING	Chukchi Sea	-9.7 ± 7.0	-4.9±5.1	-1.2 ± 1.4	-2.9±1.9	-12.6± 9.5	-14.4 ± 11.6	-6.5 ± 6.4	-3.6±2.6
	Beaufort Sea	**-3.0 ± 0.9**	**-2.9±1.1**	-1.4 ± 1.0	**-1.1±0.3**	**-3.1 ± 1.2**	-7.5+6.5	**-2.4 ± 0.7**	**-1.3±0.4**
	Canadian Archipelago	**-1.9 ± 0.9**	**-2.8±1.4**	-1.7 ± 1.1	-1.1±0.6	**-2.7 ± 1.1**	-6.6+4.2	**-2.5± 1.3**	-1.3±0.7
	Central Arctic Ocean	**-2.1 ± 1.0**	**-2.0±0.9**	-0.8 ± 0.8	**-0.8±0.3**	**-2.8 ± 1.1**	**-3.1+1.5**	-1.1 ± 0.9	-0.9±0.5
	Barents Sea	-6.9 ± 6.8	-9.3±6.3	-5.4 ± 5.8	-4.7±4.0	-10.3 ± 7.2	**-10.7+4.8**	-6.9 ± 6.6	-4.0±3.9
	Laptev Sea	**-2.8 ± 1.4**	-1.2±0.6	-0.4 ± 0.7	-0.8±0.4	-1.9 ± 1.3	-1.5±0.8	-0.5 ± 0.9	**-0.8±0.4**
	Kara Sea	-2.5 ± 4.4	-4.4±6.7	-2.0 ± 3.2	-3.4±4.0	-3.7 ± 5.3	-8.8+9.8	-1.5 ± 2.8	-4.2±4.8
	E. Siberian Sea	**-5.8 ± 2.2**	-2.2±1.2	-0.3 ± 1.1	**-1.9±0.9**	**-6.3 ± 2.3**	-3.9+3.8	-1.9 ± 1.7	-2.0±1.1

Acknowledgments:

We thank the MOSAiC science crew of the teams ECO, OCEAN and ICE, as well as the Captain and crew of RV*Polarstern* for their support during MOSAiC PS122/5 (Grant no AWI_PS122_00). We are particularly grateful to Zoe Koenig, Jacob Allerholt, Salar Karam, Michael Gallagher, Zoé Brasseur and Julia Regnery for their help with the field deployments. We thank Dr. Joo-Hong Kim, the captain, crew and science crew of RV *Araon* cruise ARA10B for their support in a preliminary study without which the autonomous AZFP buoy would not have been possible. We thank Sören Krägesky (AWI) and Angus Atkinson (PLM) for their advice. Nadine Knüppel (AWI) supported the zooplankton analysis. This study was primarily funded by the project EcoLight, as part of the bilateral Changing Arctic Ocean programme by the British National Environmental Research Council (NERC) under grant number NE/R012725/1 and the German Ministry for Education and Research (BMBF) under grant number 03V01465. A.C. was funded through the BMBF grant 03F0917A MOSAiC 3. G.C., H.F. and B.N. were also funded by the Helmholtz Association's Programme Oriented Funding Period 4 (POF-4), Topic and 6.1 and 6.3. KS was funded through NERC Grant NE/S002502/1. MG and PP were financially supported by the Ocean Frontier Institute of the Canada First Research Excellence Fund, Natural Sciences and Engineering Research Council Discovery Grant programme, ArcticNet a Network of Centres of Excellence Canada, Research Council of Norway grant 300333 Deep Impact, and Fisheries and Oceans Canada through the Atlantic Fisheries Fund. The work described in this paper has been partially funded from the European Union's Horizon 2020 research and innovation programme through the project Arctic PASSION under grant agreement No. 101003472 (MK). The instruments and buoy developments were funded by the Frontiers in Arctic Marine Monitoring (FRAM) and the Multidisciplinary Ice-based Distributed Observatory (MIDO) infrastructure programmes.

Author Information

Affiliations:

Alfred-Wegener-Institute for Polar and Marine Research, Bremerhaven, Germany

Giulia Castellani, Astrid Cornils, Hauke Flores, Mario Hoppmann, Michael Karcher, Marcel Nicolaus, Barbara Niehoff

British Antarctic Survey, Cambridge, United Kingdom

Gaelle Veyssiere, Jeremy Wilkinson

Bruncin Observation Systems, Zagreb, Croatia

Lovro Valcic

O.A.Sys - Ocean Atmosphere Systems GmbH, Hamburg, Germany

Michael Karcher

Centre for Fisheries Ecosystems Research, Fisheries and Marine Institute of Memorial University of Newfoundland and Labrador, St. John's, NL, Canada

Maxime Geoffroy, Pierre Priou

Department of Arctic and Marine Biology, The Arctic University of Norway, Tromsø, Norway

Maxime Geoffroy

Akvaplan-Niva, The Fram Centre, Tromsø, Norway

Pierre Priou

University of Plymouth, School of Geography, Earth and Environmental Sciences, Plymouth, United Kingdom

Katrin Schmidt

University of Manitoba, Centre for Earth Observation Science, Winnipeg, Canada

Julienne Stroeve

University College London, Earth Sciences Department, London, United Kingdom

Julienne Stroeve

Contributions

G.C., H.F., M.H., M.K., G.V. and J.W. conceived the research and designed the study. G.C., H.F., M.H., L.V. and J.W. developed the autonomous AZFP buoy. M.G. and P.P. advised on hydroacoustic sampling and data analysis. G.C., M.H., M.N. and K.S. performed the field work during MOSAiC. A.C., H.F., M.H., G.V., M.K, and J.W. analyzed the data. H.F. and G.V. drafted the manuscript. All authors participated in writing the paper, discussed, interpreted results, and drew conclusions.

Corresponding author

Hauke Flores [hauke.flores@awi.de]

Ethics declaration

Competing interests

The authors declare no competing interests.

Data availability

AZFP data have been submitted to the PANGAEA repository.

CTD buoy data are available at www.meereisportal.de[56] and will be available on the PANGAEA repository.

Spectral light data are available at:

Nicolaus, Marcel; Anhaus, Philipp; Arndt, Stefanie; Katlein, Christian; Krampe, Daniela; Lange, Benjamin Allen; Matero, Ilkka; Regnery, Julia; Rohde, Jan; Schiller, Martin (2021): Spectral solar radiation over and under sea ice during the MOSAiC campaign 2019/20. https://doi.org/10.1594/PANGAEA.935688[60]

Nicolaus, Marcel; Hoppmann, Mario; Tao, Ran; Katlein, Christian (2022): Spectral radiation fluxes, albedo and transmittance from autonomous measurement from Radiation Station

2020R21, deployed during MOSAiC 2019/20
https://doi.pangaea.de/10.1594/PANGAEA.948838[54] (under review)

Zooplankton data] will be available on the PANGAEA repository.

Code availability

All code used to derive the results presented in this study are available from the authors on request. Essential code will be published on Zenodo.

REFERENCES

1. Nicolaus M, Katlein C, Maslanik J, Hendricks S. Changes in Arctic sea ice result in increasing light transmittance and absorption. *Geophys Res Lett*, **39:** L24501 (2012).

2. Wassmann P, Reigstad M. Future Arctic Ocean seasonal ice zones and implications for pelagic-benthic Coupling. *Oceanography*, **24**(3)**:** 220-231 (2011).

3. Tedesco L, Vichi M, Scoccimarro E. Sea-ice algal phenology in a warmer Arctic. *Sci Adv*, **5**(5)**:** eaav4830 (2019).

4. Ardyna M, Arrigo KR. Phytoplankton dynamics in a changing Arctic Ocean. *Nat Clim Change*, **10**(10)**:** 892-903 (2020).

5. Castellani G, Veyssière G, Karcher M, Stroeve J, Banas SN, Bouman AH*, et al.* Shine a light: Under-ice light and its ecological implications in a changing Arctic Ocean. *Ambio*, **51**(2)**:** 307-317 (2022).

6. Brierley AS. Diel vertical migration. *Curr Biol*, **24**(22)**:** R1074-R1076 (2014).

7. Last Kim S, Hobbs L, Berge J, Brierley Andrew S, Cottier F. Moonlight drives ocean-scale mass vertical migration of zooplankton during the Arctic winter. *Curr Biol*, **26**(2)**:** 244-251 (2016).

8. Hobbs L, Cottier FR, Las KS, Berge J. Pan-Arctic diel vertical migration during the polar night. *Mar Ecol Prog Ser*, **605:** 61-72 (2018).

9. Geoffroy M, Daase M, Cusa M, Darnis G, Graeve M, Santana Hernández N*, et al.* Mesopelagic sound scattering layers of the high Arctic: seasonal variations in biomass, species assemblage, and trophic relationships. *Frontiers in Marine Science*, **6**(364)**:** (2019).

10. Darnis G, Hobbs L, Geoffroy M, Grenvald JC, Renaud PE, Berge J*, et al.* From polar night to midnight sun: Diel vertical migration, metabolism and biogeochemical role of zooplankton in a high Arctic fjord (Kongsfjorden, Svalbard). **62**(4)**:** 1586-1605 (2017).

11. Jónasdóttir SH, Visser AW, Richardson K, Heath MR. Seasonal copepod lipid pump promotes carbon sequestration in the deep North Atlantic. *Proceedings of the National Academy of Sciences*, **112**(39)**:** 12122-12126 (2015).

12. Darnis G, Fortier L. Zooplankton respiration and the export of carbon at depth in the Amundsen Gulf (Arctic Ocean). *J Geophys Res-Oceans*, **117:** (2012).

13. Visser AW, Grønning J, Jónasdóttir SH. *Calanus hyperboreus* and the lipid pump. *Limnol Oceanogr*, **62**(3)**:** 1155-1165 (2017).

14. Wilson RP, Puetz K, Bost CA, Culik BM, Bannasch R, Reins T*, et al.* Diel dive depth in penguins in relation to diel vertical migration of prey - whose dinner by candlelight. *Mar Ecol Prog Ser*, **94**(1)**:** 101-104 (1993).

15. Hays GC. A review of the adaptive significance and ecosystem consequences of zooplankton diel vertical migrations. *Hydrobiologia*, **503**(1-3)**:** 163-170 (2003).

16. Varpe Ø, Daase M, Kristiansen T. Food for thought: A fish-eye view on the new Arctic lightscape. *ICES Journal of Marine Science*, **72**(9)**:** 2532-2538 (2015).

17. Gjosaeter H, Wiebe PH, Knutsen T, Ingvaldsen RB. Evidence of dielvertical migration of mesopelagic sound-scatterng organisms in the Arctic. *Frontiers in Marine Science*, **4:** (2017).

18. Berge J, Geoffroy M, Daase M, Cottier F, Priou P, Cohen JH*, et al.* Artificial light during the polar night disrupts Arctic fish and zooplankton behaviour down to 200 m depth. *Communications Biology*, **3**(1)**:** (2020).

19. Hobbs L, Banas NS, Cohen JH, Cottier FR, Berge J, Varpe Ø. A marine zooplankton community vertically structured by light across diel to interannual timescales. *Biol Letters*, **17**(2)**:** 20200810 (2021).

20. Kohlbach D, Graeve M, A. Lange B, David C, Peeken I, Flores H. The importance of ice algae-produced carbon in the central Arctic Ocean ecosystem: Food web relationships revealed by lipid and stable isotope analyses. *Limnol Oceanogr*, **61:** 2027-2044 (2016).

21. Kohlbach D, Graeve M, Lange BA, David C, Schaafsma FL, van Franeker JA*, et al.* Dependency of Antarctic zooplankton species on ice algae-produced carbon suggests a sea ice-driven pelagic ecosystem during winter. *Global Change Biol*, **24**(10)**:** 4667-4681 (2018).

22. Spitschan M, Aguirre GK, Brainard DH, Sweeney AM. Variation of outdoor illumination as a function of solar elevation and light pollution. *Sci Rep-Uk*, **6**(1)**:** 26756 (2016).

23. Rabe B, Heuzé C, Regnery J, Aksenov Y, Allerholt J, Athanase M*, et al.* Overview of the MOSAiC expedition: Physical oceanography. *Elementa: Science of the Anthropocene*, **10**(1)**:** (2022).

24. Nicolaus M, Perovich DK, Spreen G, Granskog MA, von Albedyll L, Angelopoulos M*, et al.* Overview of the MOSAiC expedition: Snow and sea ice. *Elementa: Science of the Anthropocene*, **10**(1)**:** (2022).

25. Nicolaus M, Hudson SR, Gerland S, Munderloh K. A modern concept for autonomous and continuous measurements of spectral albedo and transmittance of sea ice. *Cold Regions Science and Technology*, **62**(1)**:** 14-28 (2010).

26. Skjoldal HR, Mundy P. *Large Marine Ecosystems (LMEs) of the Arctic area Revision of the Arctic LME map*, 2 edn: Akureyri, Iceland (2013).

27. Häfker NS, Teschke M, Hüppe L, Meyer B. *Calanus finmarchicus* diel and seasonal rhythmicity in relation to endogenous timing under extreme polar photoperiods. *Mar Ecol Prog Ser*, **603:** 79-92 (2018).

28. Clarke GL. Light conditions in the sea in relation to the diurnal vertical migrations of animal. Proceedings of the International Symposium on Biological sound scattering in the Ocean; 1971; Washington, DC: Maury Center Ocean Science (1971). p. 41-50.

29. Båtnes AS, Miljeteig C, Berge J, Greenacre M, Johnsen G. Quantifying the light sensitivity of Calanus spp. during the polar night: potential for orchestrated migrations conducted by ambient light from the sun, moon, or aurora borealis? *Polar Biology*, **38**(1)**:** 51-65 (2015).

30. Geynrikh A, Kosobokova K, Rudyakov YA. Seasonal variations in the vertical distribution of some prolific copepods of the Arctic Basin. *Canadian Translations of Fisheries and Aquatic Sciences*, **4925:** (1983).

31. Hirche H-J, Mumm N. Distribution of dominant copepods in the Nansen Basin, Arctic Ocean, in summer. *Deep Sea Research Part A Oceanographic Research Papers*, **39**(2)**:** S485-S505 (1992).

32. Kvile KØ, Ashjian C, Ji R. Pan-Arctic depth distribution of diapausing *Calanus* copepods. *The Biological Bulletin*, **237**(2)**:** 76-89 (2019).

33. Gradinger R, Meiners K, Plumley G, Zhang Q, Bluhm BA. Abundance and composition of the sea-ice meiofauna in off-shore pack ice of the Beaufort Gyre in summer 2002 and 2003. *Polar Biology*, **28**(3)**:** 171-181 (2005).

34. Hardge K, Peeken I, Neuhaus S, Lange BA, Stock A, Stoeck T*, et al.* The importance of sea ice for exchange of habitat-specific protist communities in the Central Arctic Ocean. *J Marine Syst*, **165:** 124-138 (2017).

35. Ehrlich J, Bluhm BA, Peeken I, Massicotte P, Schaafsma FL, Castellani G*, et al.* Sea-ice associated carbon flux in Arctic spring. *Elementa: Science of the Anthropocene*, **9**(1)**:** (2021).

36. Castellani C, Robinson C, Smith T, Lampitt RS. Temperature affects respiration rate of Oithona similis. *Mar Ecol Prog Ser*, **285:** 129-135 (2005).

37. Lischka S, Hagen W. Seasonal lipid dynamics of the copepods Pseudocalanus minutus (Calanoida) and Oithona similis (Cyclopoida) in the Arctic Kongsfjorden (Svalbard). *Marine Biology*, **150**(3)**:** 443-454 (2007).

38. Hobbs L, Banas NS, Cottier FR, Berge J, Daase M. Eat or Sleep: Availability of Winter Prey Explains Mid-Winter and Spring Activity in an Arctic *Calanus* Population. *Frontiers in Marine Science*, **7:** (2020).

39. Kohlbach D, Schmidt K, Hop H, Wold A, Al-Habahbeh AK, Belt ST*, et al.* Winter Carnivory and diapause counteract the reliance on ice algae by Barents Sea zooplankton. *Frontiers in Marine Science***:** 266 (2021).

40. Ross T, Lavery AC. Acoustic scattering from density and sound speed gradients: Modeling of oceanic pycnoclines. *The Journal of the Acoustical Society of America*, **131**(1)**:** EL54-EL60 (2012).

41. Notz DaC, SIMIP. Arctic Sea Ice in CMIP6. *Geophys Res Lett*, **47:** e2019GL086749 (2020).

42. Wassmann P. Arctic marine ecosystems in an era of rapid climate change. *Prog Oceanogr*, **90**(1-4)**:** 1-17 (2011).

43. Leu E, Soreide JE, Hessen DO, Falk-Petersen S, Berge J. Consequences of changing sea-ice cover for primary and secondary producers in the European Arctic shelf seas: Timing, quantity, and quality. *Progress in Oceanography*, **90**(1-4)**:** 18-32 (2011).

44. Hirche H-J, Niehoff B. Reproduction of the Arctic copepod *Calanus hyperboreus* in the Greenland Sea - field and laboratory observations. *Polar biology*, **16**(3)**:** 209-219 (1996).

45. Ershova EA, Kosobokova KN, Banas NS, Ellingsen I, Niehoff B, Hildebrandt N*, et al.* Sea ice decline drives biogeographical shifts of key *Calanus* species in the Central Arctic Ocean. *Global Change Biol*, **27**(10)**:** 2128-2143 (2021).

46. Darnis G, Wold A, Falk-Petersen S, Graeve M, Fortier L. Could offspring predation offset the successful reproduction of the arctic copepod *Calanus hyperboreus* under reduced sea-ice cover conditions? *Progress in Oceanography*, **170:** 107-118 (2019).

47. Gradinger RR, Bluhm BA. In-situ observations on the distribution and behavior of amphipods and Arctic cod (*Boreogadus saida*) under the sea ice of the High Arctic Canada Basin. *Polar Biol*, **27**(10)**:** 595-603 (2004).

48. Kohlbach D, Schaafsma FL, Graeve M, Lebreton B, Lange BA, David C*, et al.* Strong linkage of polar cod (*Boreogadus saida*) to sea ice algae-produced carbon: Evidence from stomach content, fatty acid and stable isotope analyses. *Progress in Oceanography*, **152:** 62-74 (2017).

49. Snoeijs-Leijonmalm P, Flores H, Sakinan S, Hildebrandt N, Svenson A, Castellani G*, et al.* Unexpected fish and squid in the central Arctic deep scattering layer. *Sci Adv*, **8**(7)**:** eabj7536 (2022).

50. Benoit-Bird KJ, Lawson GL. Ecological insights from pelagic habitats acquired using active acoustic techniques. *Annual Review of Marine Science*, **8**(1)**:** 463-490 (2016).

51. De Robertis A, Higginbottom I. A post-processing technique to estimate the signal-to-noise ratio and remove echosounder background noise. *ICES Journal of Marine Science*, **64**(6)**:** 1282-1291 (2007).

52. Ryan TE, Downie RA, Kloser RJ, Keith G. Reducing bias due to noise and attenuation in open-ocean echo integration data. *ICES Journal of Marine Science*, **72**(8)**:** 2482-2493 (2015).

53. R-Development-Core-Team. *R: A language and environment for statistical computing*. R Foundation for Statistical Computing: Vienna (2019).

54. Nicolaus M, Hoppmann M, Tao R, Katlein C. Spectral radiation fluxes, albedo and transmittance from autonomous measurement from Radiation Station 2020R21, deployed during MOSAiC 2019/20. In: PANGAEA, editor.: *PANGAEA* https://doi.pangaea.de/10.1594/PANGAEA.948838 (in review).

55. Hoppmann M, Kuznetsov I, Fang YC, Rabe B. Mesoscale observations of temperature and salinity in the Arctic Transpolar Drift: a high-resolution dataset from the MOSAiC Distributed Network. *Earth Syst Sci Data*, **14**(11)**:** 4901-4921 (2022).

56. Rabe B, Hoppmann M. Raw data of Ocean CTD buoy 2020O10. *Meereisportal* https://data.meereisportal.de/gallery/index_new.php?lang=de_DE&active-tab1=method&active-tab2=buoy&singlemap&buoyname=2020O10 (2022).

57. Gorsky G, Ohman MD, Picheral M, Gasparini S, Stemmann L, Romagnan J-B*, et al.* Digital zooplankton image analysis using the ZooScan integrated system. *Journal of Plankton Research*, **32**(3)**:** 285-303 (2010).

58. Picheral M, Colin S, Irisson JO. EcoTaxa - A tool for the taxonomic classification of images. [cited 2022] Available from: http: //ecotaxa.obs-vlfr.fr/; (2017)

59. Katlein C, Schiller M, Belter HJ, Coppolaro V, Wenslandt D, Nicolaus M. A New Remotely Operated Sensor Platform for Interdisciplinary Observations under Sea Ice. *Frontiers in Marine Science*, **4:** (2017).

60. Nicolaus M, Anhaus P, Arndt S, Katlein C, Krampe D, Lange BA*, et al.* Spectral solar radiation over and under sea ice during the MOSAiC campaign 2019/20. *PANGAEA* https://doi.org/10.1594/PANGAEA.935688 (2021).

61. Castellani G, Losch M, Lange BA, Flores H. Modeling Arctic sea-ice algae: Physical drivers of spatial distribution and algae phenology. *J Geophys Res-Oceans*, **122**(9)**:** 7466-7487 (2017).

62. Dix M, Bi D, Dobrohotoff P, Fiedler R, Harman I, Law R*, et al.* CSIRO-ARCCSS ACCESS-CM2 model output prepared for CMIP6 CMIP. *Earth System Grid Federation* https://doi.org/10.22033/ESGF/CMIP6.2281 (2019).

63. Jungclaus J, Bittner M, Wieners K-H, Wachsmann F, Schupfner M, Legutke S*, et al.* MPI-M MPIESM1.2-HR model output prepared for CMIP6 CMIP. *Earth System Grid Federation* https://doi.org/10.22033/ESGF/CMIP6.741 (2019).

64. Brovkin V, Wieners K-H, Giorgetta M, Jungclaus J, Reick C, Esch M*, et al.* MPI-M MPIESM1.2-LR model output prepared for CMIP6 C4MIP. *Earth System Grid Federation* https://doi.org/10.22033/ESGF/CMIP6.748 (2019).

65. Yukimoto S, Koshiro T, Kawai H, Oshima N, Yoshida K, Urakawa S*, et al.* MRI MRI-ESM2.0 model output prepared for CMIP6 AerChemMIP. *Earth System Grid Federation* https://doi.org/10.22033/ESGF/CMIP6.633 (2019).

66. Rutan DA, Kato S, D.R: D, Rose FG, Nguyen L, Caldwell TE*, et al.* CERES Synoptic Product: Methodology and Validation of Surface Radiant Flux. *Journal of Atmospheric and Oceanic Technology*, **32:** 1121 - 1143 (2015).

67. Perovich D, T. Grenfell, B. Light, J. Richter-Menge, T. Tucker. Wavelength-integrated Albedos. Version 1.0. UCAR/NCAR. 2007).

68. Jakobsson M, Mayer LA, Bringensparr C, Castro CF, Mohammad R, Johnson P*, et al.* The International Bathymetric Chart of the Arctic Ocean Version 4.0. *Scientific Data*, **7**(1)**:** 176 (2020).

69. Soreide JE, Leu E, Berge J, Graeve M, Falk-Petersen S. Timing of blooms, algal food quality and *Calanus glacialis* reproduction and growth in a changing Arctic. *Global Change Biol*, **16**(11)**:** 3154-3163 (2010).

Supplementary Files

This is a list of supplementary files associated with this preprint. Click to download.

- FloresZooplanktonLongerDeepersuppl.pdf